

Synthesis and Characterization of solid electrolyte and electrode material for all-solid-state Li batteries.

A thesis

submitted to

Indian Institute of Science Education and Research Pune in partial fulfilment of the requirements for the BS-MS Dual Degree Programme

by

Kiran Anne Roy

(20151076)



Indian Institute of Science Education and Research Pune

Dr Homi Bhabha Road,

Pashan, Pune 411008, INDIA.

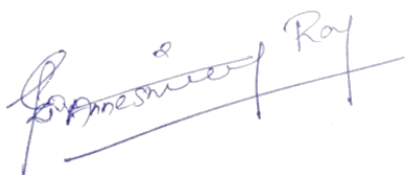
April 2020

Supervisor: **Prof. Satichchandra B Ogale**

All rights reserved


Certificate

This is to certify that this dissertation entitled **Synthesis and Characterizations of solid electrolytes for all-solid-state Li batteries** towards the partial fulfilment of the BS-MS dual degree programme at the Indian Institute of Science Education and Research, Pune represents study/work carried out by **Kiran Anne Roy** at Indian Institute of Science Education and Research under the supervision of **Prof. Satichchandra B Ogale**, Professor, Department of Physics during the academic year 2019-2020.



Kiran Anne Roy

Registration number:20151076



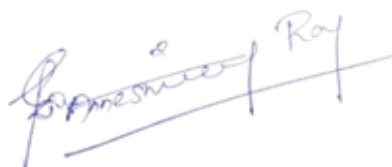
Prof. Satichchandra B Ogale

Supervisor

This thesis is dedicated to my parents.....

Declaration

I hereby declare that the matter embodied in the report entitled **Synthesis and Characterizations of solid electrolytes for all-solid-state Li batteries** are the results of the work carried out by me at the Department of Physics, Indian Institute of Science Education and Research, Pune, under the supervision of **Prof. Satichchandra B Ogale** and the same has not been submitted elsewhere for any other degree.



Kiran Anne Roy

(20151076)



Prof. Satichchandra B Ogale

Supervisor

Acknowledgement

I express my deepest gratitude to God the Almighty for his blessings so that I could accomplish my thesis entitled “Synthesis and Characterizations of solid electrolytes for all-solid-state Li batteries” as the requirement for BSMS dual degree from IISER Pune.

Foremost, I would like to thank my supervisor Prof. Satishchandra Ogale for allowing me to do my thesis study and for his valuable guidance, support and patience during this period. I am also thankful for my fellow lab mates for providing a lively working environment. I must make a special mention for Kingshuk Roy for providing me immense help and guidance to complete this project.

I am thankful to Mr Anil, Mr Yathish and Mr Sudhir to help me obtain the FESEM data. Also, Mr Prashant for helping me procure the TEM data. I thank the Department of Chemistry, teaching and non- teaching staffs for helping me directly as well as indirectly during my academic journey. I should thank IISER Pune for laying out an extremely good academic atmosphere.

I extend my gratefulness towards my family, especially my parents for giving birth to me in the first place and supporting me emotionally throughout my life. I thank all my friends scattered around the globe for their e-mails, phone calls, visits, texts, thoughts and well-wishes, and being there for me. I am indebted to all my friends here and my roommate for helping, listening and supporting me throughout this journey.

Kiran Anne Roy

Table of contents

1. INTRODUCTION	12
1.1 Historic development of Solid-state batteries.....	12
1.2 Working principle of Li-ion battery.....	13
1.3 Mechanism of transport in Solid-state electrolytes.....	13
1.4 Components of a Lithium-ion battery.....	13
1.4.1 Cathode.....	13
1.4.2 Anode.....	14
1.4.3 Binder.....	14
1.4.4 Separator.....	15
1.4.5 Electrolyte.....	15
1.5 Cubic LLZO- a garnet type electrolyte.....	16
2. Experimental techniques	17
2.1 Materials and methods.....	17
2.1.1 Chemicals and materials.....	17
2.1.2 Synthesis of pyrolyzed carbon fibers.....	17
2.1.3 Synthesis of Al-doped LLZO.....	17
2.1.4 Electrospinning method.....	17
2.2 Analysis techniques.....	19
2.2.1 X-ray diffraction (XRD).....	19

2.2.2 Field Emission Scanning Electron Microscopy (FESEM).....	20
2.2.3 Transmission Electron Microscopy (TEM).....	21
2.2.4 Selected Area Electron Diffraction (SAED).....	23
2.2.5 Raman spectroscopy.....	24
2.3 Electrode preparation and coil cell fabrication.....	26
2.4 Electrochemical characterization.....	27
Galvanostatic charge-discharge measurement.....	27
3. Results and discussion.....	30
3.1 Structural characterization.....	30
3.1.1 PXRD.....	30
3.1.1.1 PXRD of Al-doped LLZO.....	30
3.1.1.2 PXRD of the pyrolyzed carbon fibers.....	31
3.1.2 FESEM.....	31
3.1.2.1 FESEM of Al-doped LLZO.....	31
3.1.2.2 FESEM of pyrolyzed carbon fibers.....	32
3.1.3 TEM.....	34
3.1.3.1 TEM of Al-doped LLZO.....	34
3.1.3.2 TEM images of pyrolyzed carbon fibers.....	34
3.1.4 Raman spectroscopy.....	36
3.2 Electrochemical characterization.....	37
4. Summary and prospects.....	41

5. References.....42

Table of figures

Figure no:	Title	Page
1.1	Structure of cubic LLZO	16
2.1	Schematic for illustration of Electrospinning technique.	18
2.2	Schematic for illustration of Bragg's diffraction.	20
2.3	Schematic for illustration of Field Emission Scanning Electron Microscopy.	21
2.4	Schematic for illustration of Transmission Electron Microscopy	22
2.5	Schematic for illustration of Selected area electron diffraction	24
2.6	Schematic for illustration of the Jablonski diagram of quantum energy transitions for Rayleigh and Raman scattering	25
2.7	Schematic for illustration of Raman spectrometer	26
2.8	Schematic for the illustration of coil cell fabrication	27
3.1	XRD pattern of Al-doped LLZO	30
3.2	XRD pattern of the pyrolyzed carbon fibers	31
3.3	FESEM images of Al-doped LLZO	32
3.4.1	FESEM images of PVA pyrolyzed polymer	32
3.4.2	FESEM images of PVP pyrolyzed polymer	33
3.4.3	FESEM images of pyrolysed polymer fibers where both PVP and PVA polymers are equally mixed	33

3.5	TEM images of Al-doped LLZO	34
3.6.1	TEM images of pyrolyzed PVA carbon fibers	35
3.6.2	TEM images of pyrolyzed PVP polymer fibers	35
3.6.3	TEM images of pyrolysed polymer fibers where both PVP and PVA polymers are equally mixed	36
3.7	Raman spectrum of the carbon fibers, PVA, PVP and PVP+PVA	36
3.8	Electrochemical measurements of pyrolyzed PVA polymer	37
3.9	Electrochemical measurements of pyrolyzed PVP polymer	38
3.10	Electrochemical measurements of pyrolyzed PVP + PVA polymer	39
3.11	Stability plot comparison of PVA, PVP and PVP+PVA	40

Abstract

Researches are being done constantly in Lithium-ion battery to improve its properties like the capacity, stability and rate. Electrolytes are being studied over the years to enhance the properties of batteries. Solid-state electrolytes were discovered which paved way to a more safe, compact and cost-efficient batteries. $\text{Li}_7\text{La}_3\text{Zr}_2\text{O}_{12}$ (LLZO) is a garnet type oxide electrolyte having high conductivity. The properties of LLZO were improved by incorporating or doping various elements on them. Doping with the elements like Ga, Al etc. helps in developing a cubic phase in them which has high conductivity. Here, Aluminium is doped on LLZO to develop a cubic phase. Chemical and physical characterizations were done to observe the morphology, crystallinity and the phase formed.

Three different polymer solutions were made using PVA, PVP and PVA+PVP, electrospun and pyrolyzed. The characterizations like XRD, FESEM, TEM and Raman spectroscopy were performed on respective samples. The samples were used in making three respective electrodes and fabricated into Lithium-ion coin cells. Charge- discharge measurements were conducted on the coin cells to study its electrochemical properties. Based on the properties, the material can be chosen to be used in electrodes. The Al-doped LLZO and any of the pyrolyzed carbon fiber chosen by its chemical and electrochemical properties can be used in a battery by altering its properties by various methods.

Chapter 1

INTRODUCTION

The increasing demand for a sustainable source of energy led to the development of energy harvesting and energy storage systems. Batteries gained wide attention as it is one of the efficient means of energy storage. The development of batteries led to the discovery of Lithium-ion batteries which has many advantages to make it preferable over the other batteries. It has a high energy density, low self-discharge and relatively low maintenance. The battery contains an electrochemical system which uses an electrolyte. Recent years had led to the development of solid-state electrolytes due to the safety concerns raised by the use of liquid electrolyte. These are compact, minimal and preclude the need of separators which add to the volume of the battery.

1.1 Historic development of Solid-state batteries

Solid-state conductors carry an old history when the conducting property in heated solids such as Ag_2S and PbF_2 was discovered by Faraday. But the solid-state electrolytes were considered to be incorporated in batteries only by 1960s. In the 1960s, Sodium-ion transport was observed in β -alumina and used to develop high-temperature sodium-sulfur batteries. Other inorganic materials like Ag_3SI and RbAg_4I_5 were also used as solid-state ionics. In 1973, poly (ethylene oxide) (PEO) which is an organic polymer also fell into the category of solid-state ionics. In the early twenties, more studies were done based on the understanding of the ionic transport mechanism, superionic conductors and enhancing the performance of the electrical devices having solid electrolytes. The thought of incorporating solid-state electrolytes at ambient temperature was driven by the safety concerns of using a liquid electrolyte in Lithium-ion batteries. The short-circuiting or overcharging of the lithium-ion battery using a liquid electrolyte is one of a major problem. The solid-state electrolyte falls into two categories: (i) Lithium ion-conductive polymers (ii) Inorganic Lithium-ion conductive ceramics. The Lithium-ion conductive ceramics was developed in the 1990s after the discovery of lithium phosphorous oxynitride (LIPON). After the discovery of LIPON, many inorganic conductive materials such as garnet type,

NASICON type, sulfide type and perovskite-type materials were discovered. By 2000, solid-state electrolyte batteries using gaseous and liquid cathodes were developed.

1.2 Working principle of Li-ion battery

On charging, when an external voltage is being applied across the battery the Lithium ions move from cathode to anode through an electrolyte while the electrons move from cathode to anode through an external circuit. On discharge, the Lithium ions stored in the anode move towards the cathode through the electrolyte and the electrons move from anode to cathode through an external circuit.

1.3 Mechanism of transport in Solid-state electrolytes

The ionic transport mechanism in solid-state electrolytes is through the distribution and contribution of defects. The Frenkel and Schottky point defects which include the diffusion transport and the vacancy mechanisms contribute to the ionic transport. But, in some materials, the absence of defects still contributes to the high ionic conductivity. These materials have a structure which comprises of two sublattices. A sublattice consisting of mobile ions and a crystal framework having immobile ions. The equivalent sites for the mobile ions to occupy should be much higher than that of the number of the mobile ions. The barrier energy for migration should be much low for the ions to hop easily and there should be a connection between the available sites to form a continuous path of diffusion. In polymer electrolytes, a segmental motion of the polymer chain occurs at a temperature above the glass transition temperature and the sites are created for the ions to hop by coordinating with the polar groups.

1.4 Components of a Lithium-ion battery

1.4.1 Cathode

The cathode is the positive electrode of the battery. Lithium ions move from the cathode to the anode of the battery on charging. Therefore, the lithium ions are released by the cathode. Lithium is unstable in its elemental form; therefore, lithium oxides are used as the cathode. To make the material active, transition metal oxides are used

as the cathode. A cathode determines the voltage and the capacity of the battery. When a higher number of lithium ions are released into the electrolyte, higher the capacity. Hence a higher potential difference is being developed between the cathode and the anode. There are different types of cathode materials like spinel, layered, tavorite and olivine based on the arrangement of atoms and crystal structure. Examples are Lithium Cobalt Oxide (LCO) which is a layered transition metal oxide with capacity 274 mAh g⁻¹, high voltage and high stability. Lithium Nickel Oxide (LNO) is another transition metal oxide cathode. Polyanionic compounds are also used as cathode materials. (XO₄)³⁻, X-(Si, S, P, Mo) where the polyanions occupy the lattice position. These materials increase the work potential of the cathode thus increasing its power density. LiFePO₄ is one such polyanionic cathode material.

1.4.2 Anode

The anode is the negative electrode of the battery. The stability and life of the battery is determined by the anode. The material used in anode should be having high cycling stability and high gravimetric capacity. Even though Lithium has a high specific capacity, it cannot be used as anode material due to the Lithium dendrite formation and reaction with moisture. Therefore, various other materials could be used as anode material based on its ability to store Lithium ions on charging. Graphite is used as an anode material. It stores lithium by intercalation between its two planes. It has the capacity of 372 mAh g⁻¹. Another type of anode material is the conversion anode where the anode material changes from an ion to metal. Transition metal sulfides are one such conversion electrodes which on intercalation changes to metal and Li₂S. It shows a capacity of about 600mAh g⁻¹. The alloys like Mg, Al, Si, Sb, Sn, Ag etc. can also be used as an anode material.

1.4.3 Binder

Binder plays an important role in actively mixing the materials used in the electrode together and then adhering them to the current collector. Binders like Polyvinylidene Fluoride (PVDF) and Carboxymethyl cellulose (CMC) is used commonly for this process.

1.4.4 Separator

Separator is the barrier between the anode and the cathode. It determines the safety of the battery. It is a porous film placed between an anode and a cathode which avoids the electrical contact between them thereby preventing the short circuit. The material is semi-permeable in such a manner that it only allows the ions to pass through and not the electrons. The binder has thermal stability and is chemically inactive. The common binders used are synthetic resins like polypropylene and polyethylene.

1.4.5 Electrolyte

Electrolyte is the medium of Lithium-ion transport between the electrodes in the battery. It should have a wide temperature window, high ionic conductivity, high ionic selectivity, excellent chemical compatibility and wide electrochemical stability window. The electrolytes are of two types: (i) liquid electrolytes (ii) solid electrolytes. The liquid electrolyte solvates the ions from one electrode and desolvates at the other electrode. Lithium hexafluorophosphate in ethylene carbonate is a commonly used liquid electrolyte in a Lithium-ion battery. The shortcomings of safety issues caused by the liquid electrolyte is overcome by the solid electrolyte. The solid electrolytes are of various types such as the organic polymer electrolytes, inorganic electrolytes like the garnet, sulfide, NASICON and perovskite.

1.5 Cubic LLZO- a garnet type electrolyte

Cubic $\text{Li}_7\text{La}_3\text{Zr}_2\text{O}_{12}$ (LLZO) is a garnet type oxide electrolyte with high mechanical and thermal stability. Cubic LLZO is formed only at high temperature. The stable low-temperature LLZO has a tetragonal phase. The cubic phase in LLZO is made stable at all temperatures with Aluminum on the Lithium site. Cubic LLZO has a high ionic conductivity of around $10^{-3} \text{ S cm}^{-1}$. It has a wide potential window of about 6V. The chemical stability of cubic LLZO against the lithium and the mechanical strength makes this a better solid electrolyte to be used in lithium-ion batteries.

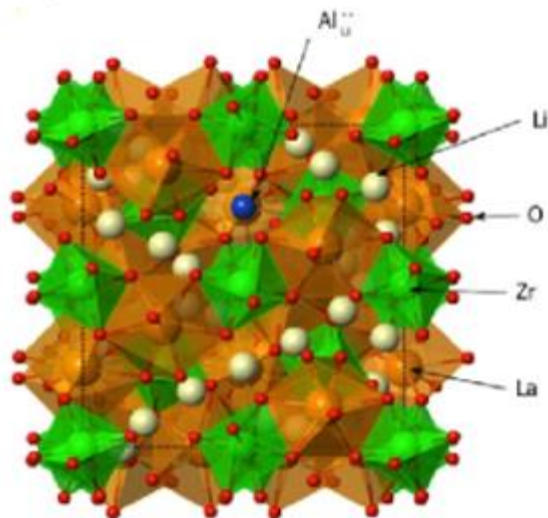


Figure 1.1: Structure of cubic LLZO

(Reference - <https://doi.org/10.1021/acs.chemmater.5b03854>)

LLZO exists in two polymorphic structures, a cubic and a tetragonal structure. The tetragonal structure exists in the lower temperature with an ordered arrangement of Lithium ions. There is less or no defects. It has dodecahedral LaO_8 polyhedral structures which are of two types and a ZrO_6 octahedral structure. Li-ion occupies in three different sites: tetrahedral (8a), distorted octahedral 32g and 16f sites.

The cubic structure has no ordered arrangement of Lithium ions. There is a presence of defects exhibited by the disordered arrangement of Lithium ions. It has a space group of $Ia-3d$ and contains an eight-fold coordinated LaO_8 and a six-fold coordinated ZrO_6 octahedral structure. The Li-ions occupy the interstitial sites having octahedral (48g), tetrahedral (24d) and distorted four-fold (96h) sites.

Chapter 2

Experimental techniques

2.1 Materials and methods

2.1.1 Chemicals and materials

Polyvinyl alcohol $[\text{CH}_2\text{CH}(\text{OH})]_n$, Polyvinyl pyrrolidone $[\text{C}_6\text{H}_9\text{NO}]_n$, water, 19.8wt% LiOH, 52.5wt% La_2O_3 , 26.5wt% ZrO_2 , 1.2wt% Al_2O_3 , Conducting carbon, N-Methyl-2-pyrrolidone (NMP), Ethylene carbonate, Lithium hexafluorophosphate (LiPF_6), Lithium metal, copper foil, Celgard 2300 membrane.

2.1.2 Synthesis of pyrolyzed carbon fibers

Three different polymer solutions are made. The following solutions are:

- (i) Polyvinyl alcohol (PVA) of 1gm dissolved in 10ml of water.
- (ii) Polyvinyl pyrrolidone (PVP) of 1gm dissolved in 10ml of water.
- (iii) PVA and PVP of 5gm each is dissolved in 10ml water.

Three of the polymer solutions were dissolved in water by heating at about 60°C . These solutions were electrospun at 20kV. The fibers were collected and pyrolyzed from room temperature to 900°C at a rate of $10^\circ\text{C}/\text{min}$. It was held at this temperature for 2hrs and then allowed to cool.

2.1.3 Synthesis of Al-doped LLZO

19.8wt% LiOH, 52.5wt% La_2O_3 , 26.5wt% ZrO_2 and 1.2wt% Al_2O_3 was mixed by ball milling for 5 hours. The mixture was calcined at 800°C for 12 hours. The calcined mixture was ground and pressed into pellets using a KBr die set of 10mm. These pellets were then sintered at 1000°C for 36hrs. It is then ball milled for an hour and crushed into powder.

2.1.4 Electrospinning method

Electrospinning is a process which utilizes the electrohydrodynamic phenomenon using voltage to synthesize carbon fibers from the polymer solution. This technique involves the following set of components: (1) high voltage source (2) syringe (3) collector. A high

voltage is applied at the tip of the syringe to produce an electric field between the syringe tip and the collector. The charge is accumulated at the tip of the syringe where the drop of the solution comes out. Hence the electrostatic repulsion in the drop becomes higher than the surface tension and the drop at the tip of the syringe deforms to a conical shape called the Taylor's cone. A jet is formed at the tip of the cone and is ejected toward the collector with the electric field. As a result, the polymer fibers are formed at the collector. These fibers have a diameter ranging from 10 nm to a few micrometers. The pump which pumps the polymer solution from the syringe is set in such a manner that it allows a constant supply of solution at a constant rate. The morphology of the fibers can be altered by various arrangements using the electrospinning technique.

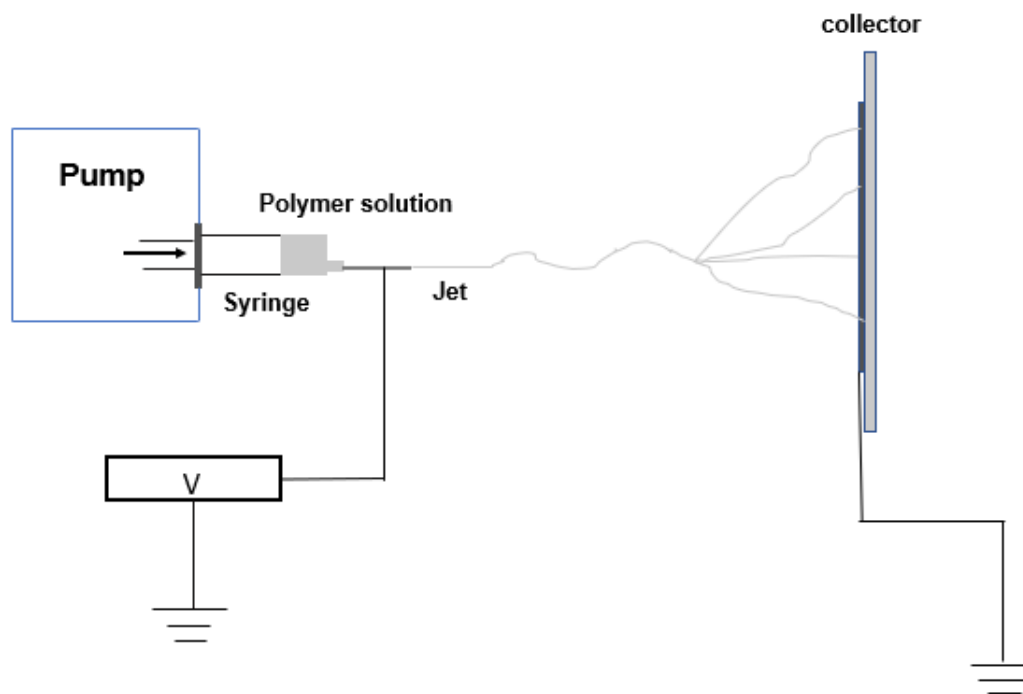


Figure2.1: Schematic for illustration of Electrospinning technique.

2.2 Analysis techniques

2.2.1 X-ray diffraction (XRD)

XRD is a rapid analytical and non-destructive method used for the identification of phases and the unit cell dimensions of a crystal structure. It provides the details about the lattice parameters, size of the crystal and the anisotropic growth found in the material. X-ray is a high energy electromagnetic radiation having a wavelength between 0.01 to 10nm. The interplanar distances in the crystal lattice has the same order of magnitude as that of the X-ray. Therefore, X-ray is used for the crystal determination. A cathode-ray tube generates X-rays and is filtered to produce a monochromatic beam of radiation. This monochromatic beam is then concentrated by collimation and is focused on the sample. When this incident on the crystal, diffraction patterns in different directions are observed based on the electron cloud density of the crystal. The diffracted beams add up and cancel each other undergoing a constructive and destructive interference respectively. The constructive interference occurs when it satisfies the Bragg's law.

$$n\lambda = 2d \sin\theta$$

n- Order of diffraction

λ - Wavelength of the incident X-ray beam.

θ - Angle of scattering

d- inter-planar distance

PXRD was carried out using Bruker D8-Advance X-ray Diffractometer (Germany) with Cu α (wavelength – 1.5418 Å)

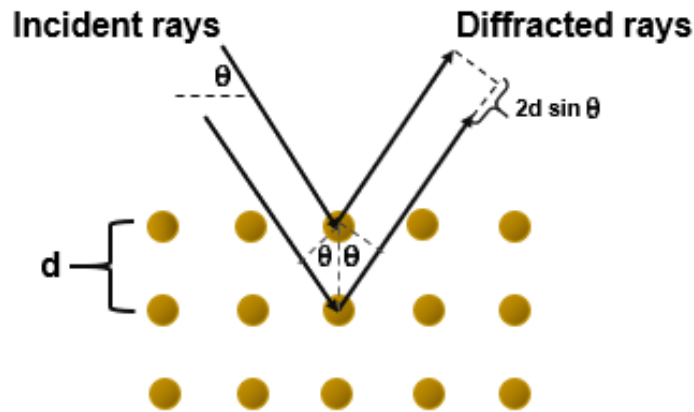


Figure:2.2 Schematic for illustration of Bragg's diffraction.

All the diffraction directions are obtained by scanning the sample through a range of 2θ angles. Each material has its unique d-spacings. The conversion of diffraction peaks to d-spacings will help us identify the material.

2.2.2 Field Emission Scanning Electron Microscopy (FESEM)

FESEM is performed to observe tiny surface topography over the entire area of the sample. FESEM is a microscopic technique which involves negatively charged electrons instead of light. FESEM provides a clear and less electrostatically distorted high-resolution image compared to SEM (Scanning Electron Microscopy). Electrons are ejected from a field emission cathode at the electron gun and is accelerated in a high electric field. The primary electrons ejected are focused to a narrow beam within the vacuum column by the electronic lenses. This primary electron bombards the sample causing the emission of secondary electrons from the sample. The velocity and angle of the secondary electrons can be related to the surface structure of the sample.

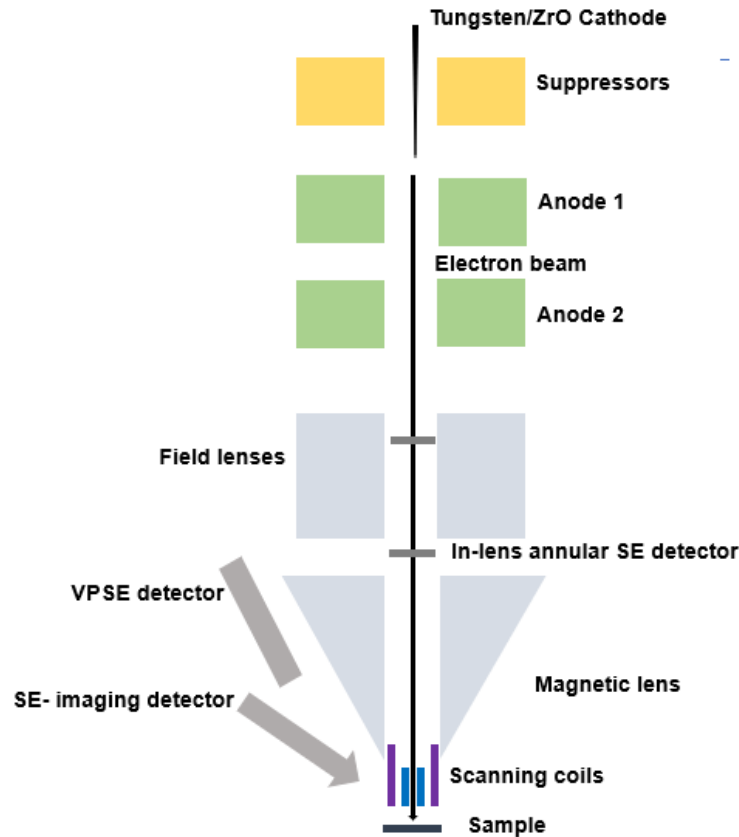


Figure:2.3 Schematic for illustration of Field Emission Scanning Electron Microscopy.

The detector collects the secondary electrons and process them into an electric signal. The signal is then amplified and transformed into a high-quality image. Electron loss is prevented at the detector by keeping at a high vacuum (10^{-7} torr). The high-resolution image is limited by diffractions or aberrations. The spatial resolution of an electron microscope is more than an optical microscope. The resolution limit in an electron microscope is around 0.017nm. FESEM was done using FEI Nova Nano 450 SEM.

2.2.3 Transmission Electron Microscopy (TEM)

TEM is a microscopy technique where an image is produced when a beam of electrons is transmitted through the sample. TEM and light microscope works on the same principle but electrons are used in TEM instead of light. The resolution of the light microscope is limited by the wavelength of light while electrons have a much smaller wavelength and

can produce high magnified high-resolution images. A high energy electron beams are shone on the sample and the interaction between the atoms of the sample and the electrons provides information about the crystal structure, morphology, grain boundaries, crystallization and the presence of strain in the sample. High-resolution TEM is used to analyze the quality, shape, size and density of the quantum wells and dots. TEM requires ultra-thin sample for the transmission of electrons through the sample. Therefore, carbon-coated TEM grids are used which are electron semipermeable. The high energy narrow beam of electrons emitted from the cathode of the electron gun is accelerated towards the anode. The beam is restricted by a condenser aperture which cuts off high angle electrons. This narrow beam strikes the ultra-thin sample and part of it transmitted based on its thickness and electron transparency. The transmitted beam is focused by the objective lens into an image. The image then passes through the projector lens for enlarging. Light which is visible to the human eye is generated when it strikes the phosphor screen. TEM and HRTEM were done using JEM 220 fs Joel 200kV.

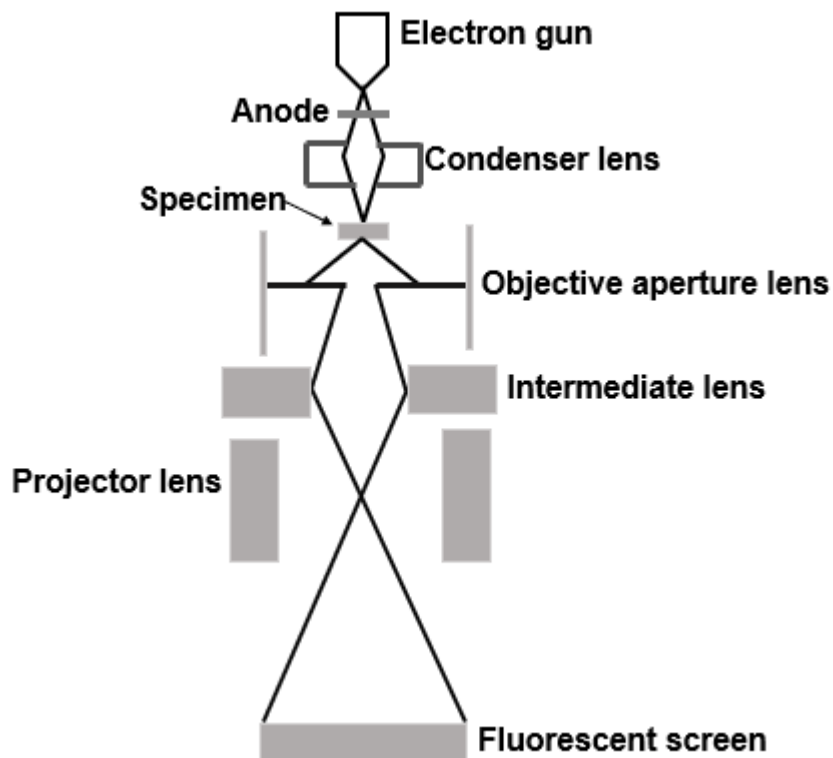


Figure 2.4 Schematic for illustration of Transmission Electron Microscopy

2.2.4 Selected Area Electron Diffraction (SAED)

Selected area electron diffraction (SAED) is a Transmission electron microscopy technique used to obtain diffraction patterns of the electron beam which is scattered by the sample. By Bragg's law, the electrons are elastically scattered by the sample. Therefore, the diffraction spots can be indexed to identify the sample phases and their structures. The SAED selects the sample within its aperture of 0.5-1 μm . SAED is used to obtain information on the sample structure like space group, crystalline symmetry and unit cell parameters. A parallel electron beam interacts with the sample. To limit the volume of the sample that adds to the diffraction, SAED aperture is maintained at the image plane of the lower objective lens. The diffraction pattern obtained is analyzed by the software. The diffraction pattern can be simulated by inputting the test parameters following the kinematic theory of electron diffraction. The spot intensity is proportional to the structure factor. The d-spacing between the spots is calculated by combining the Bragg's law and the geometric relation in reciprocal space.

$$2d \sin\theta = \lambda \text{ (Bragg's law)}$$

$$\tan 2\theta = D/L \text{ (geometric relation in reciprocal space)}$$

At a very small diffraction angle, $\sin\theta$ is equal to $\tan 2\theta$. Therefore, the equation obtained for calculating the d-spacing between the spots is

$$d = D/(\lambda L)$$

θ – diffraction angle

d – space between the planes

D – distance between the spots

λ – wavelength of the beam

L – length of the camera

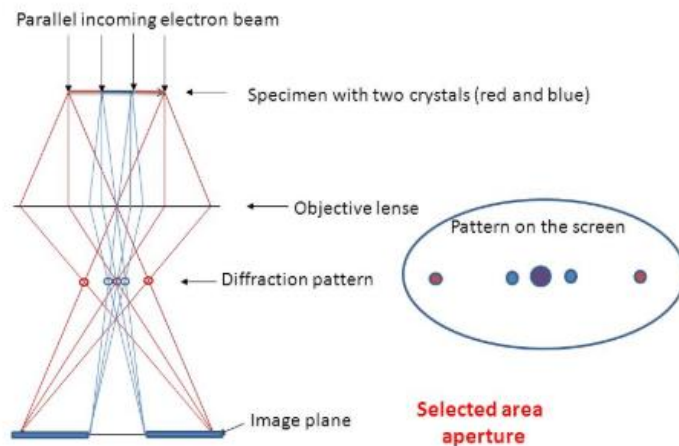


Figure 2.5 Schematic for illustration of Selected area electron diffraction
 (Reference - <https://www.slideserve.com/osman/the-transmission-electron-microscope>)

2.2.5 Raman spectroscopy

Raman spectroscopy is a technique in which the inelastic scattering of light is used to observe the vibrational states of the molecules in the sample. Raman spectroscopy provides the structural and chemical information of the sample which is the characteristic fingerprint of the sample. Therefore, this allows in identifying the chemical species with similar structures. When the electromagnetic light strikes the molecule, it interacts with them by polarizing its molecular electron cloud and transferring the energy of the photon. Hence, the molecule leaves to a higher virtual energy state. This is a very short-lived state as the photon is re-emitted immediately and the molecule relaxes back to a lower energy state. The relaxing back of the molecule to a lower energy state can occur in three ways. Firstly, when the molecule comes down to its ground state emitting a photon having the same energy as that of the incident photon. This is called elastic scattering or Rayleigh scattering. Secondly, when the molecule comes down to a lower energy state emitting a photon of lesser energy than that of the incident photon. This is called Stokes Raman scattering. Thirdly, the molecule is already in an excited state and when the incident photon strikes, it goes to a high virtual state. The relaxation of the molecule back to a

lower energy state emits a photon of higher energy than that of the incident photon. At room temperature, most molecules are found in its ground state, so Stokes shifts are mostly considered in Raman measurements. The Raman spectroscopy was performed using the LabRAM HR, HorbiaJobinYvon.

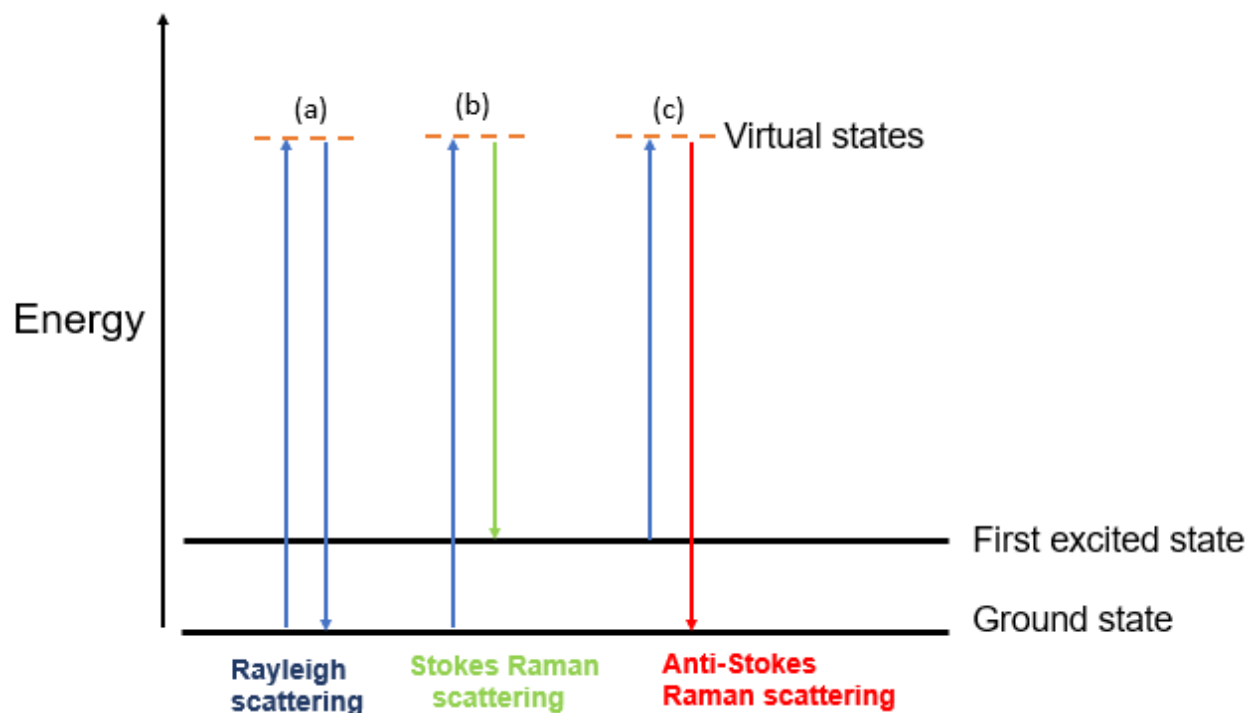


Figure 2.6 Schematic for illustration of the Jablonski diagram of quantum energy transitions for Rayleigh and Raman scattering

The Raman spectrometer has three primary components: (i) excitation source (ii) detector (iii) sampling apparatus.

The Raman spectrometer measures the wavelength or frequency shifts, therefore a monochromatic source should be used for excitation. When the excitation source is not sharp, errors are produced in the Raman shifts. More powerful Raman signals are produced at a shorter wavelength. Lasers are a good source of excitation. Hence an extremely stable laser with narrow bandwidth and shorter wavelength is used. A The monochromatic laser beam is focused towards the sample. The Raman shifted light

produced by the sample is filtered out by the dichroic mirror from the laser light and focused towards the CCD detector.

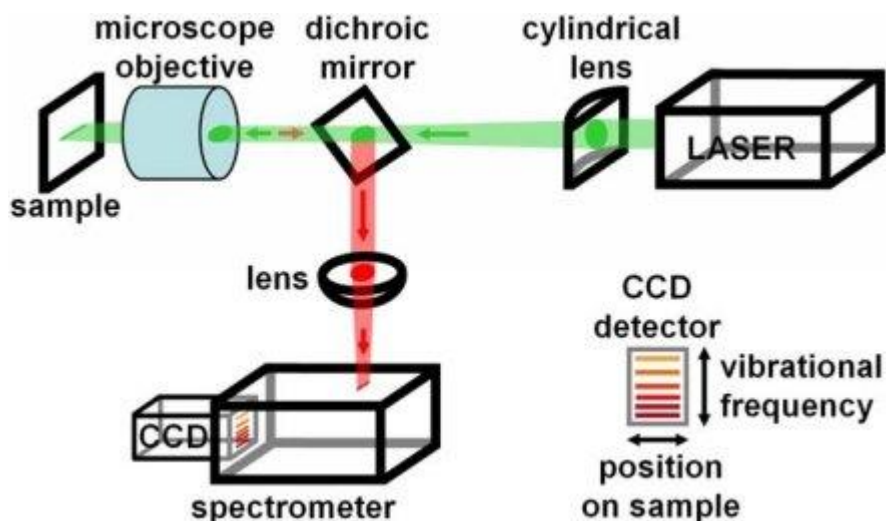


Figure 2.7 Schematic for illustration of Raman spectrometer

(Reference -https://www.researchgate.net/figure/Schematic-of-Raman-spectrometer-The-displayed-set-up-focuses-the-illuminating-laser_fig1_49677464)

2.3 Electrode preparation and coil cell fabrication

The electrode was prepared by mixing the sample (14mg), conduction carbon (4mg) and PVDF binder (2mg) in the ratio 7:2:1 respectively in NMP solvent. The samples used for preparing the electrodes are:

- (i) Pyrolyzed PVA
- (ii) Pyrolyzed PVP
- (iii) Pyrolyzed PVP+PVA

Three electrodes were made. Each electrode was made by mixing the respective sample with the conducting carbon, PVDF binder and NMP solvent physically using a mortar and

pestle to form a paste. The paste was coated evenly on the copper foil and allowed to dry in the oven at 70°C. This coated copper foil after being dried is punched into 1 cm diameter small wafers. The active material loading of electrodes were 2.45 to 2.53 mg cm⁻². Lithium metal was used as the counter electrode. 1 Molar LiPF₆ in 1:1 v/v DMC/EC was used in the coin cell as the electrolyte. Separator used was Celgard-2300 membrane. The coin cell was fabricated using a spacer, electrode, separator and electrolyte in the following manner given in Figure 2.8

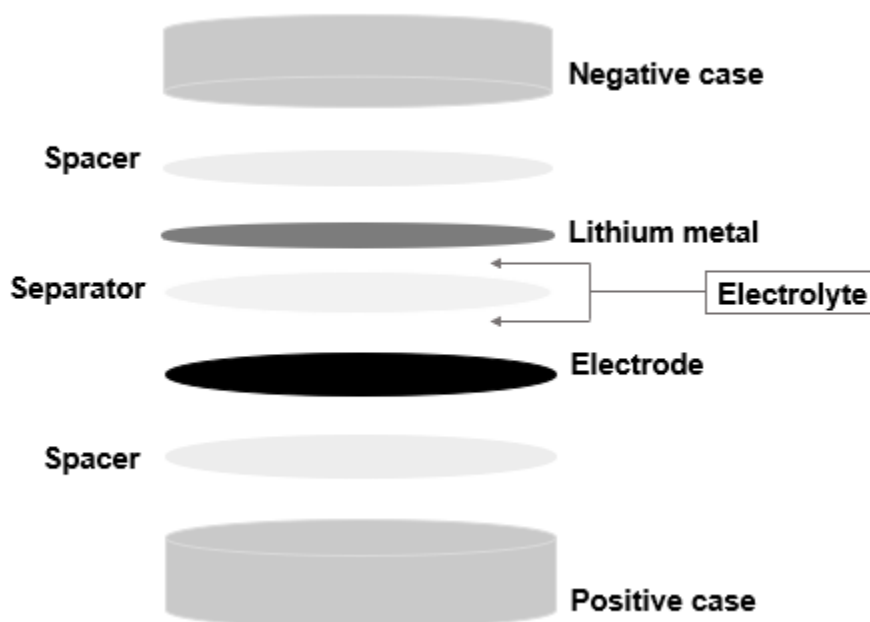


Figure 2.8 Schematic for the illustration of coin cell fabrication

2.4 Electrochemical characterization

Galvanostatic charge-discharge measurement

Galvanostatic charge-discharge measurement provides information on the cycling stability, efficiency, specific capacity and specific energy. The current is kept constant thereby measuring the voltage as the function of time.

The capacity of a battery is the total amount of electrons transferred either during charge or discharge.

The **theoretical capacity** of a battery is calculated by Faraday's law.

$$\text{Theoretical capacity} = \frac{nF}{3.6 * Mw} \text{ mAh g}^{-1}$$

n – number of charge carriers

F – Faraday's constant in C mol⁻¹

Mw – Molecular weight of the active material in g mol⁻¹

The **specific capacity** is calculated from the Voltage-time curve of the charge-discharge measurement. The specific capacity is less than the theoretical capacity.

$$\text{Specific Charge/Discharge capacity} = \frac{I * t}{m}$$

I – Current in milliamperes (mA)

t – Time in hour

m – Mass of the active material in grams

Energy density is the amount of energy stored in a unit volume of a battery. It is the maximum amount of charge that can be stored in a battery

$$\text{Energy density} = I * t * V \text{ Whkg}^{-1}$$

I – current in mA

t – Time in hours

V – Voltage

Power density is the rate at which the energy can be delivered by a battery

$$P = E/ t$$

P – power

E – Energy

t – Time

Power density is expressed in $W\ kg^{-1}$

Coulombic efficiency is the ratio of total amount of charge drawn from the battery to the total amount of charge given to the battery over a full cycle. When the coulombic efficiency is below 100%, it indicates the loss of capacity in the cell. This capacity loss might occur due to the active material dissolution in the electrolyte, ions getting trapped in the anode material or the side reactions during charge/discharge cycle.

Cycling stability explains the durability of the battery. The specific capacity against the number of cycles is plotted to observe the cycling stability. It can be observed that the capacity gets degraded with time due to the side reactions, electrolyte degradation, desolation of the active material in the electrolyte.

Rate capability measures the capability of an active material to retain its capacity at various current densities. This is measured by varying the current densities and taking the charge-discharge measurement

Chapter 3

Results and discussion

3.1 Structural characterization

3.1.1 PXRD

3.1.1.1 PXRD of Al-doped LLZO

The powder x-ray diffraction pattern of the final sintered product is given in the figure3.1

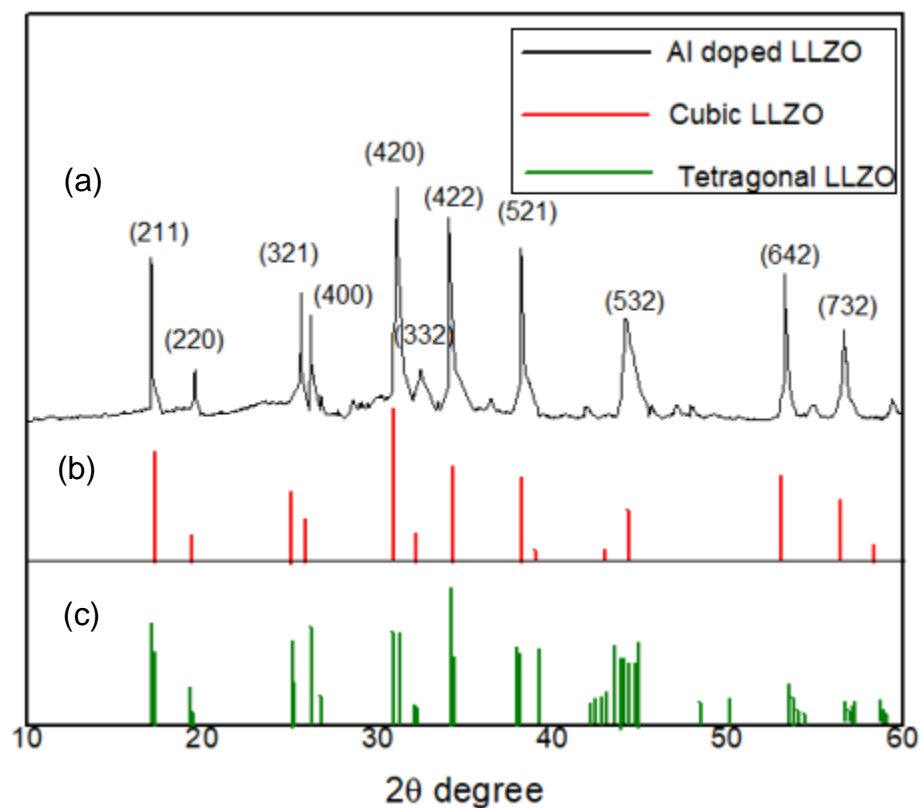


Figure3.1 (a) XRD pattern of Al-doped LLZO; (b) JCPDS 45-109 of Cubic LLZO;
(c) JCPDS 80-0457 of Tetragonal LLZO

From the figure3.1, it can be found that the XRD pattern of the Al-doped LLZO matches with the JCPDS of cubic LLZO. Hence, a cubic phase is formed in Al-doped LLZO which has a high conductivity than that of the tetragonal phase.

3.1.1.2 PXRD of the pyrolyzed carbon fibers.

The XRD pattern of the pyrolyzed carbon fibers given in the figure 3.2. The XRD pattern showing the amorphous nature of the polymers

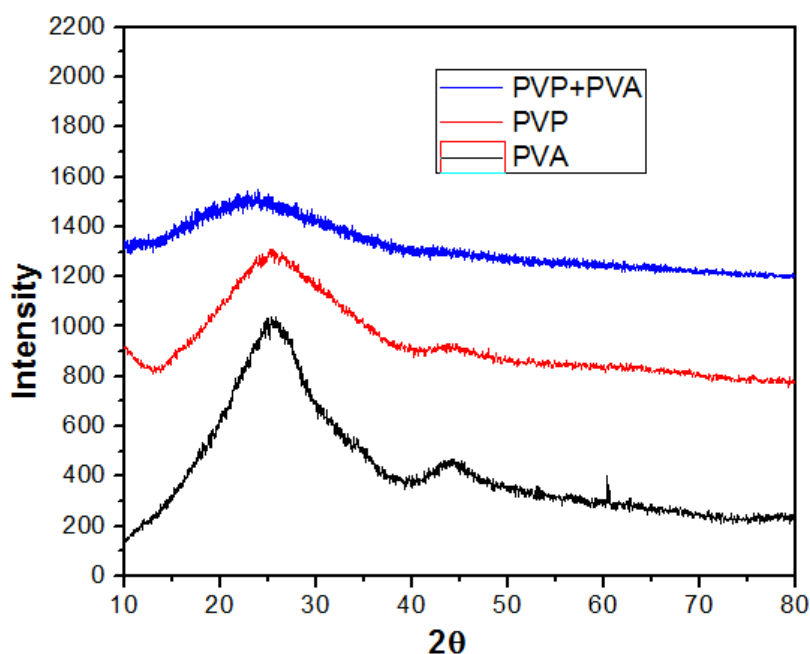


Figure3.2 XRD pattern of the pyrolyzed carbon fibers

3.1.2 FESEM

3.1.2.1 FESEM of Al-doped LLZO.

The FESEM of Al-doped LLZO given in the figure3.3. The FESEM images show the presence of layered morphology in Al-doped LLZO.

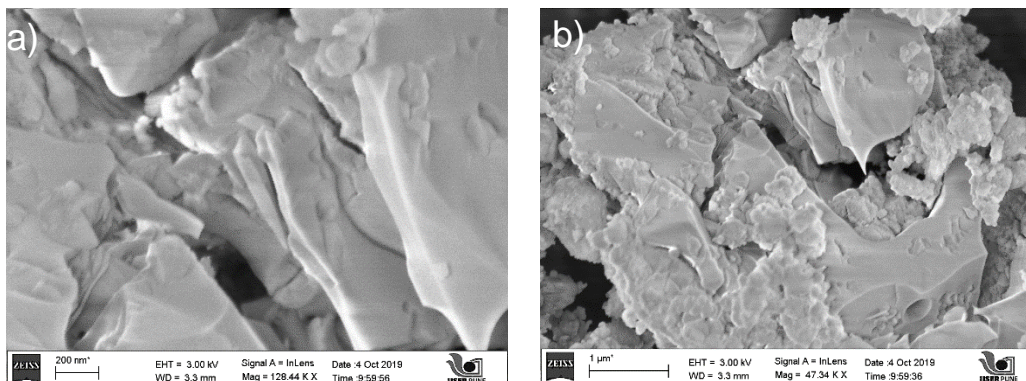


Figure3.3 FESEM images of Al-doped LLZO

3.1.2.2 FESEM of pyrolyzed carbon fibers

The FESEM images of the three respective pyrolyzed polymers are given in the figure3.4.1, figure3.4.2 and figure3.4.3.

(i) **PVA**

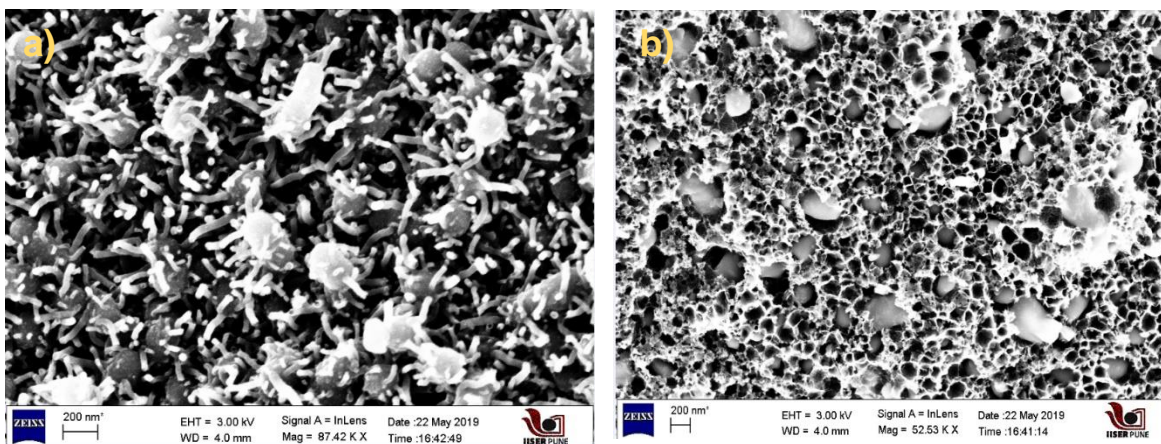


Figure3.4.1 FESEM images of PVA pyrolyzed polymer

The FESEM images show the presence of pores. The cluster of nanofibers seen as white bulk is the cluster of nanofibers formed due to the covalent bond making and breaking between the polymers

(ii) PVP

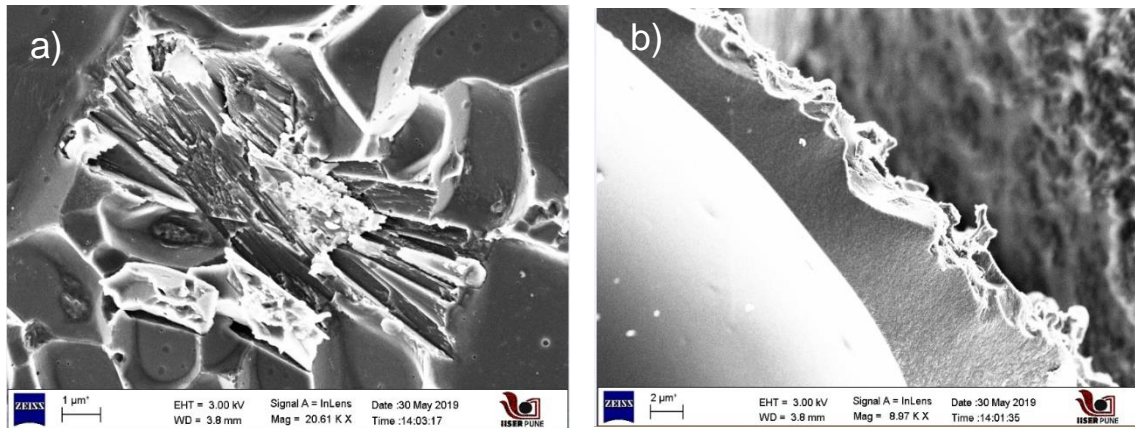


Figure3.4.2 FESEM images of PVP pyrolyzed polymer

(iii) PVP+PVP

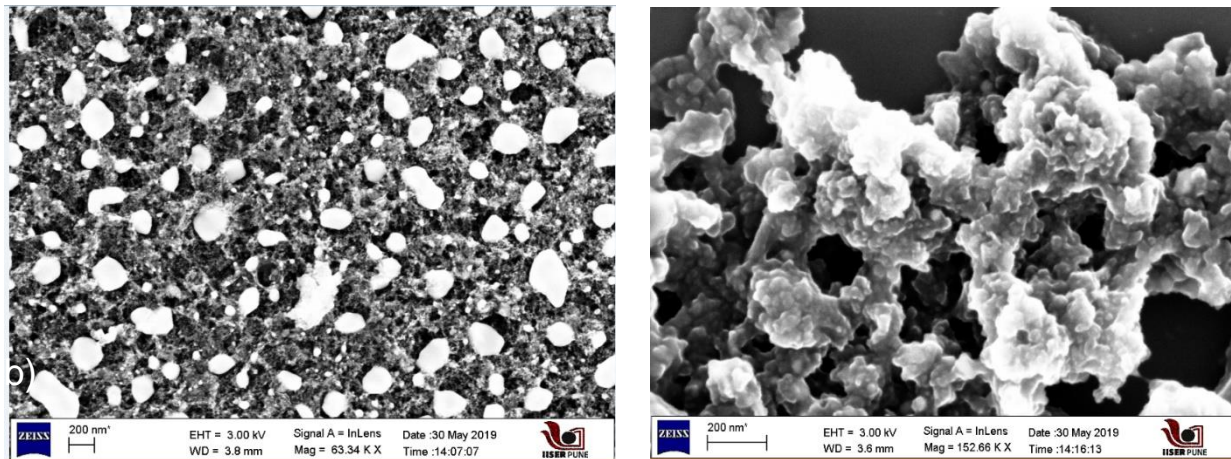


Figure3.4.3 FESEM images of pyrolysed polymer fibers where both PVP and PVA polymers are equally mixed

Figure3.4.3 shows the presence of pores. This is due to the presence of PVA

3.1.3 TEM

3.1.3.1 TEM of Al-doped LLZO

The TEM images of Al-doped LLZO are given in the figure3.5. The TEM image shows the presence of grains. The inter-planar spacing is 0.24 nm which corresponds to the (521) hkl plane in Al-doped LLZO. The SAED pattern in the figure3.5(b) shows a cubic polycrystalline structure

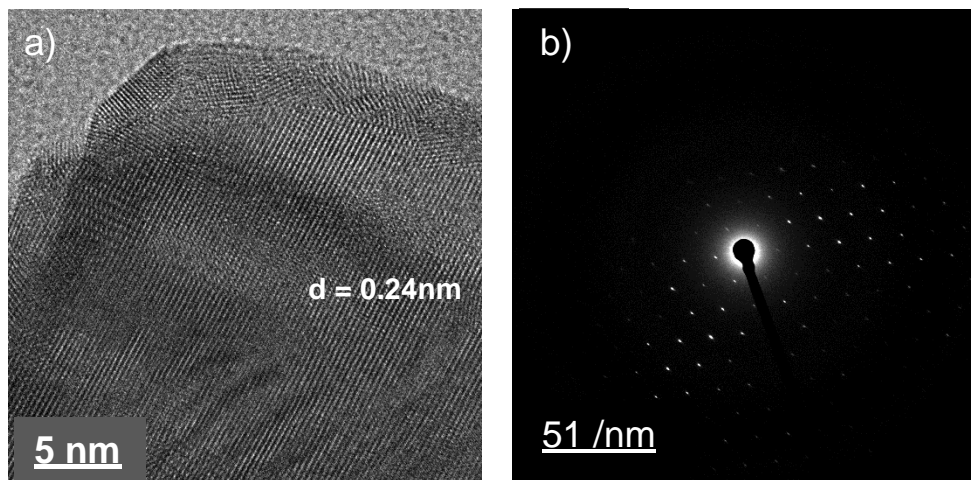


Figure3.5 TEM images of Al-doped LLZO

3.1.3.2 TEM images of pyrolyzed carbon fibers.

The TEM images of the three respective pyrolyzed polymers are given in the figure3.6.1, figure3.6.2 and figure3.6.3.

(i) PVA

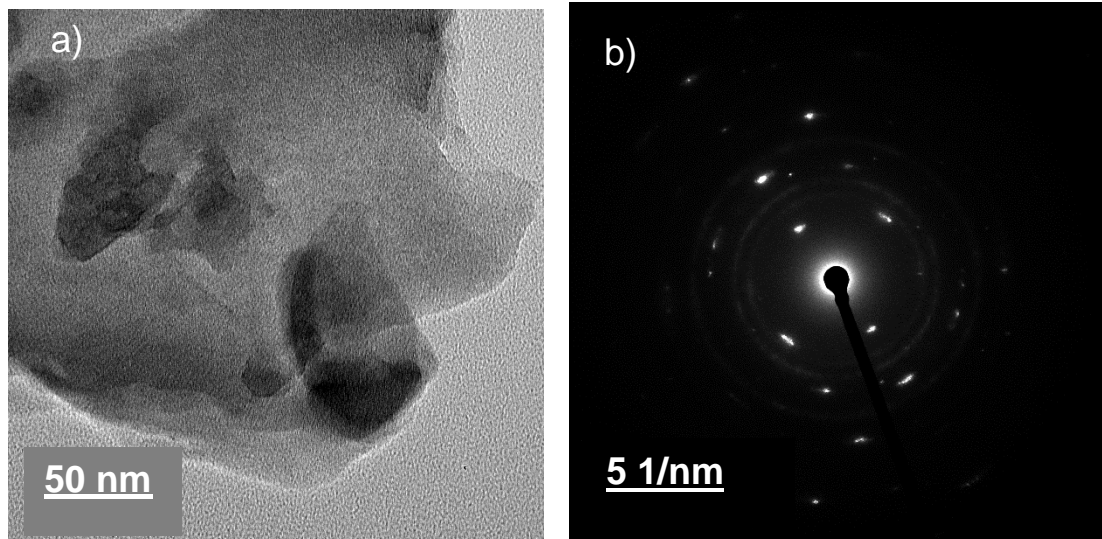


Figure.3.6.1 TEM images of pyrolyzed PVA carbon fibers

(ii) PVP

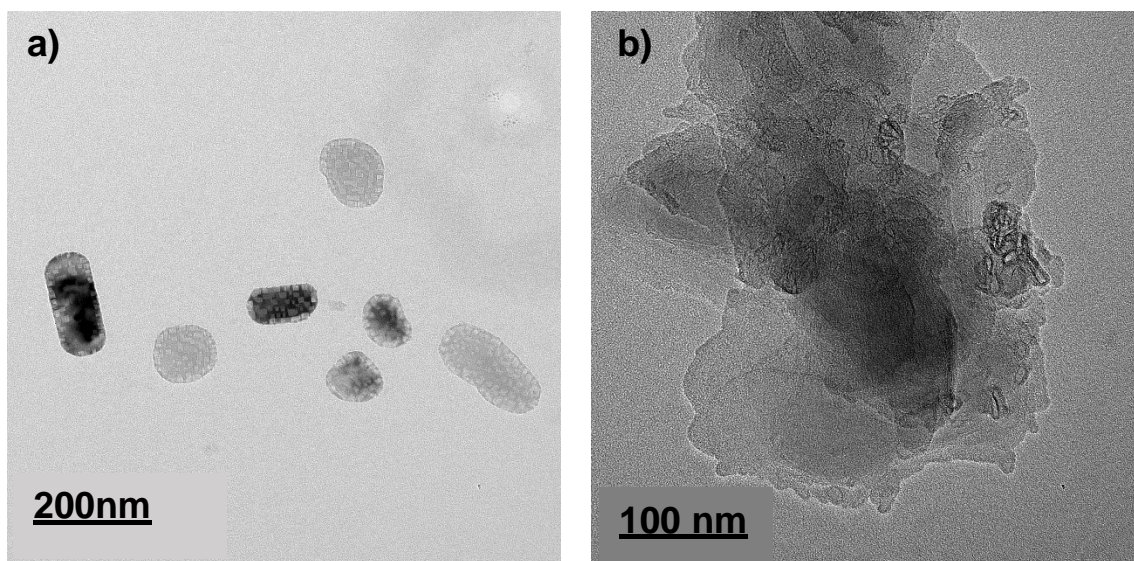


Figure3.6.2 TEM images of pyrolyzed PVP polymer fibers

(iii) PVP +PVP

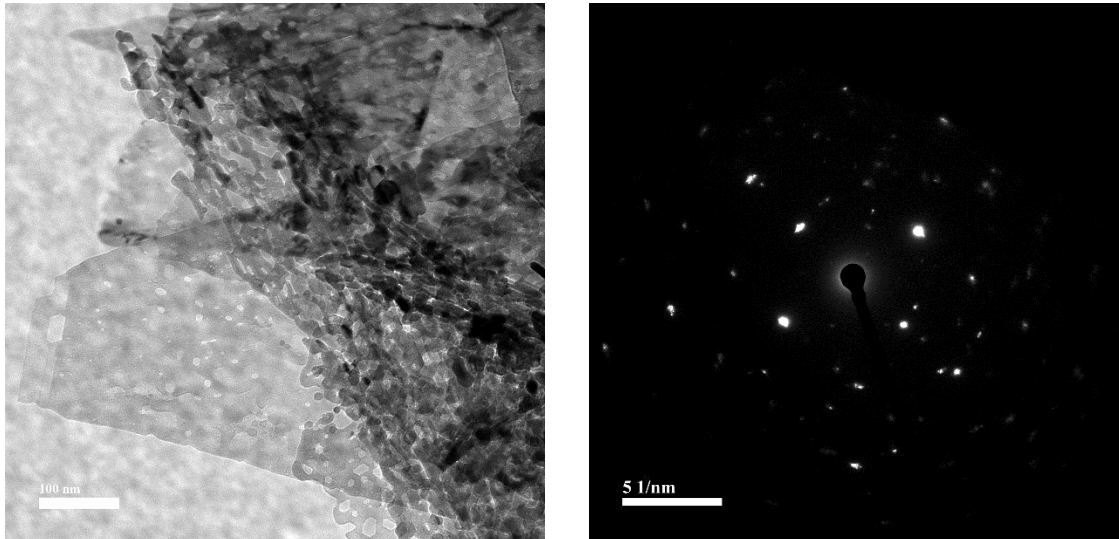


Figure3.6.3 TEM images of pyrolyzed polymer fibers where both PVP and PVA polymers are equally mixed

3.1.4 Raman spectroscopy

Figure 3.7 shows the Raman spectroscopy of the three pyrolyzed carbon fibers.

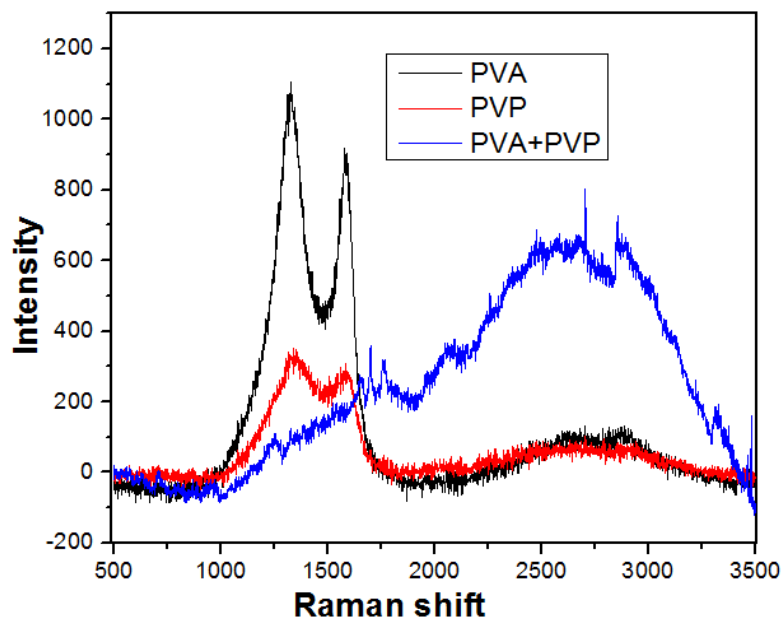


Figure.3.7 Raman spectrum of the carbon fibers, PVA, PVP and PVP+PVA

3.2 Electrochemical characterization

Galvanostatic charge-discharge measurements

The capacity measurements were done on the Lithium-ion coin cells. The electrodes made by coating the three pyrolyzed polymer samples respectively is used in Lithium-ion coin cell battery for testing.

(i) PVA

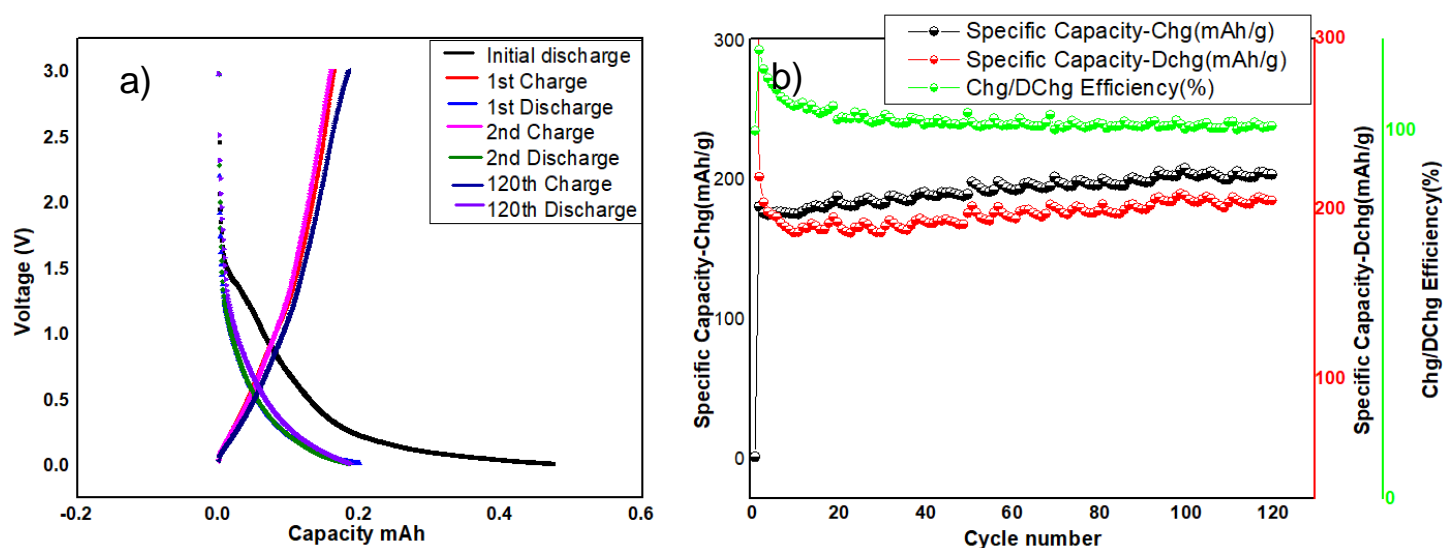


Figure 3.8 Electrochemical measurements of pyrolyzed PVA polymer at 0.091 mA

(a) The charge-discharge curve of PVA; (b) Stability curve of PVA

The charge-discharge measurements of pyrolyzed PVA polymer was done at 0.091 mA with an initial discharge capacity of 0.474 mAh. This capacity reduces to 0.167 mAh at the end of 120 cycles. Mass of the active material is 0.91 mg.

(ii) PVP

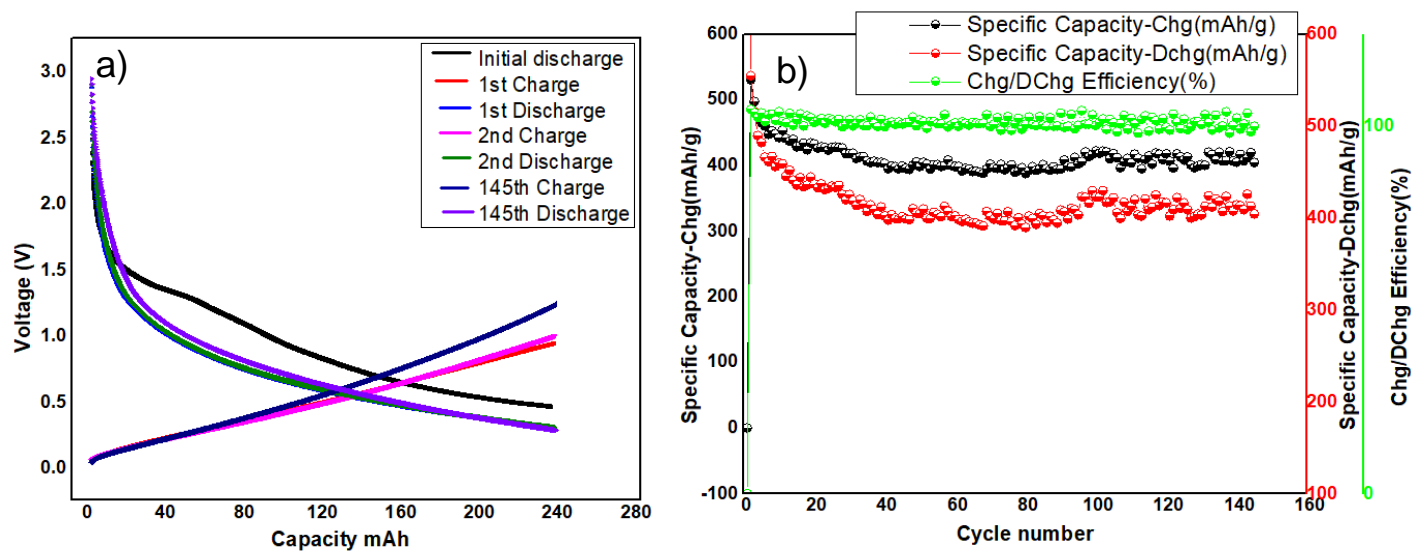


Figure 3.9 Electrochemical measurements of pyrolyzed PVP polymer at 0.077mA

(a) Charge-discharge curve of PVP; (b) Stability curve of PVP

The charge-discharge measurements of the pyrolyzed PVP polymer was done at 0.077mA for 145 cycles. The initial discharge capacity was found to be 235 mAh reduces to 0.266 mAh within 145 cycles. Mass of the active material is 0.77mg.

(iii) PVP+PVA

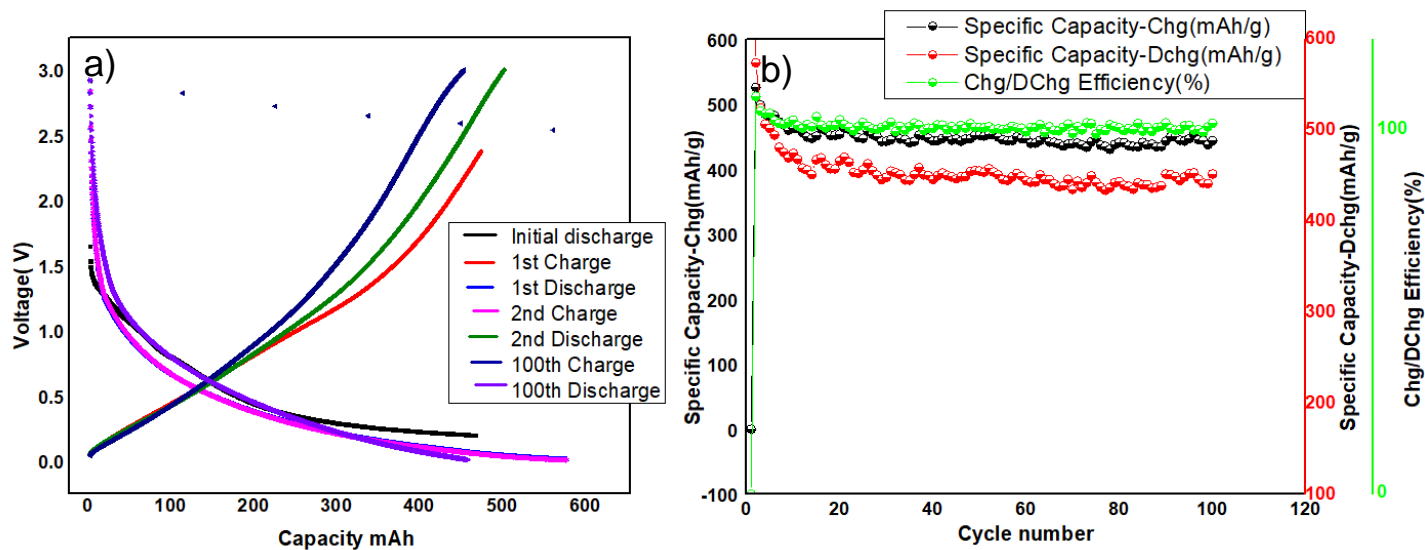


Figure 3.10 Electrochemical measurements of pyrolyzed PVP + PVA polymer at 0.126 mA
(a) The charge-discharge curve of PVA+PVP; (b) Stability curve of PVA+PVP

The charge-discharge measurements of the PVP+PVP polymer was done at 0.126mA. The initial discharge capacity was observed to be 454 mAh and reduces to 0.247 mAh at the end of 100 cycles. Mass of the active material is 0.63mg.

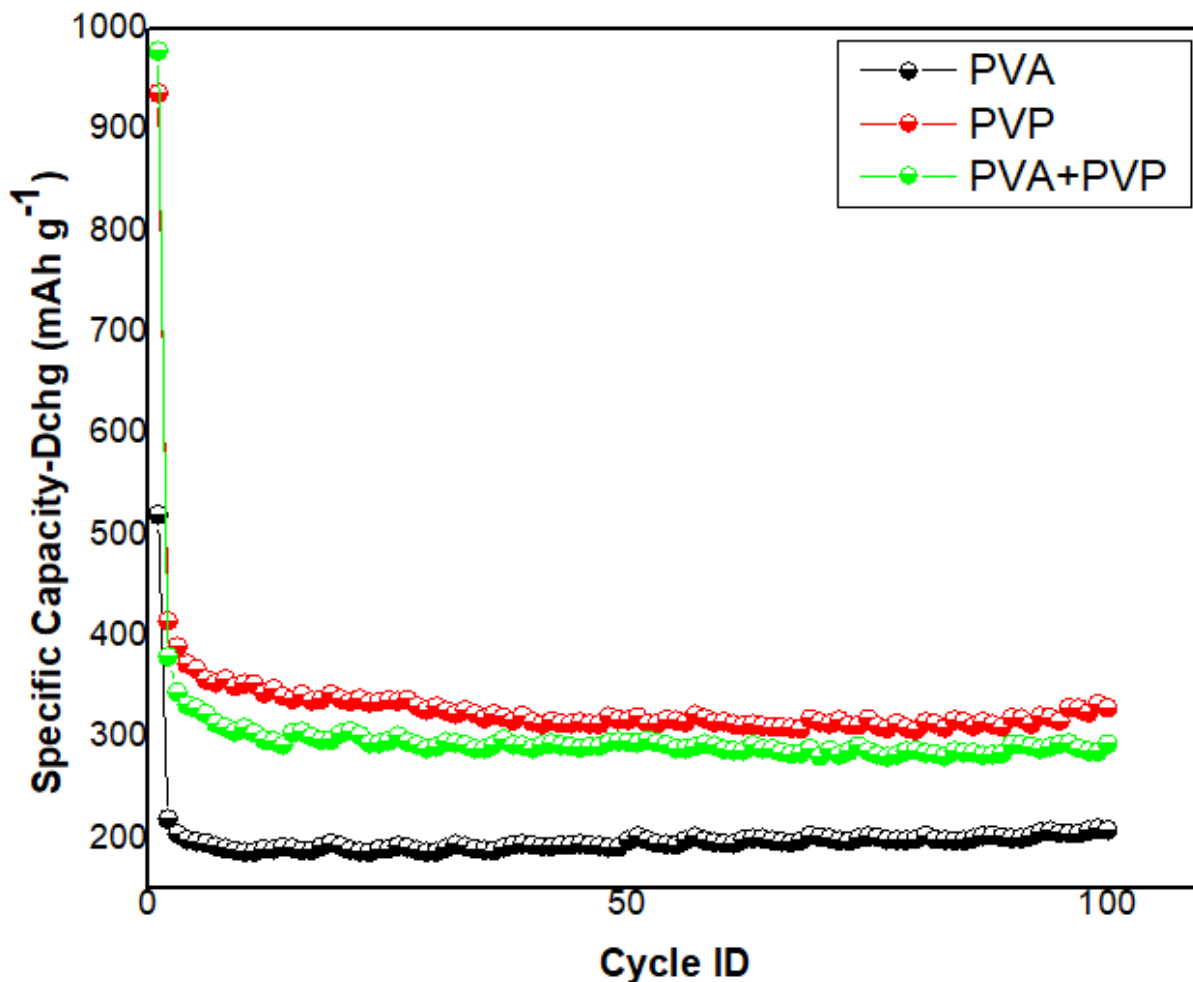


Figure 3.11 Stability plot comparison of PVA, PVP and PVP+PVA

Figure 3.11 shows the comparison of stability curves of PVA, PVP and PVA+PVP pyrolyzed polymers. It was seen that the initial discharge capacity is high for PVP+PVA polymer but it reduces to a specific capacity of 392 mAh g⁻¹ (Mass of the active material is 0.63 gm). PVA shows a stable discharge curve when compared with the other three pyrolyzed polymers. But the capacity of the PVA polymer is very less. PVP also shows a huge drop in its capacity by the end of 145 cycles. It was observed that there is a huge reduction in capacity when PVP polymer is added.

Chapter 4

Summary and prospects

To summarize the project, Al-doped LLZO solid electrolyte was synthesized by solid-state reaction. The XRD pattern obtained for the material confirms that the phase formed is cubic. Other characterizations like FESEM, TEM and SAED were also done to examine the morphology and crystalline structure of the material. However, electrochemical characterization was not done to study the electrochemical properties of the material

The three polymer fibers PVA, PVP and PVA+PVP were synthesized by electrospinning method and then pyrolyzed under high temperature. The chemical and physical characterization techniques like XRD, FESEM, TEM, SAED and Raman spectroscopy were performed on the pyrolyzed fibers. The galvanostatic charge-discharge measurements were also performed on the coin cells having an electrode coated with each of the pyrolyzed fibers respectively. It was observed that the PVP and PVP+PVA showed a huge reduction in initial discharge capacity after some cycles. PVA was stable among the three but the capacity is very less.

Effort was to combine both the materials, that is to fabricate a Lithium-ion coin cell using the Al-doped electrolyte and the pyrolyzed carbon fiber coated electrode.

Future plans:

- To combine the oxide electrolyte, Al-doped LLZO with a sulfide electrolyte to increase its stability.
- To perform electrochemical characterization techniques on Al-doped LLZO.
- To explore other materials to be incorporated in the carbon fibers to improve its capacity and stability.
- To study the effects of bulk modulus on the solid electrolyte material.

References

1. S. Yu , R.D Schmidt , R. Garcia-Mendez. Elastic Properties of the Solid Electrolyte $\text{Li}_7\text{La}_3\text{Zr}_2\text{O}_{12}$ (LLZO). *Chem. Mater.* 2016, 28, 1, Pages 197-206
2. A. Manthiram, X. Yu and S. Wang. Lithium battery chemistries enabled by solid-state electrolytes. *Nature Reviews, Material* Volume 2, Article Number 16103.
3. F. Langer, I. Bardenhagen, J. Glenneberg. Microstructure and temperature-dependent lithium ion transport of ceramic–polymer composite electrolyte for solid-state lithium ion batteries based on garnet-type $\text{Li}_7\text{La}_3\text{Zr}_2\text{O}_{12}$. *Solid State Ionics*, Volume 291, August 2016, Pages 8-13.
4. J. Zheng , M. Tang ,YY. Hu . Lithium-Ion Pathway within $\text{Li}_7\text{La}_3\text{Zr}_2\text{O}_{12}$ -Polyethylene Oxide Composite Electrolytes. *Angew Chem. Int. Ed.* 2016, 55, Pages 12538 –12542.
5. N. Rosenkiewitz, J. Schuhmacher, M. Bockmeyer. Nitrogen-free sol–gel synthesis of Al-substituted cubic garnet $\text{Li}_7\text{La}_3\text{Zr}_2\text{O}_{12}$ (LLZO). *Journal of Power Sources* ,Volume 278, 15 March 2015, Pages 104-108
6. T. Thompson, J. Wolfenstein, J. L. Allen. Tetragonal vs. cubic phase stability in Al – free Ta doped $\text{Li}_7\text{La}_3\text{Zr}_2\text{O}_{12}$ (LLZO). *Journal of Materials Chemistry*, Issue 33, 2014, Pages 13431-13436
7. R. Wagner, G.J. Redhammer, D. Rettenwander. Crystal Structure of Garnet-Related Li-Ion Conduct $\text{Li}_{7-3x}\text{Ga}_x\text{La}_3\text{Zr}_2\text{O}_{12}$: Fast Li-Ion Conduction Caused by a Different Cubic Modification. *Chem Mater.* 2016 Mar 22; 28(6), Pages 1861–1871.
8. C. Liu, Z. G. Neale, G. Cao. Understanding electrochemical potentials of cathode materials in rechargeable batteries. *Materialstoday*, Volume 19, Issue 2, March 2016, Pages 109-123
9. S. Ohta, T. Kobayashi, J. Seki. Electrochemical performance of an all-solid-state lithium-ion battery with garnet-type oxide electrolyte. *Journal of Power Sources*, Volume 202, 15 March 2012, Pages 332-335

10. J. G. Kim, B. Son, S. Mukherjee. A review of lithium and non-lithium based solid-state batteries Sources. *Journal of Power Sources*, Volume 282, 15 May 2015, Pages 299-322
11. W. Xue, Y. Yang, Q. Yang, Y. Liu. The effect of sintering process on lithium ionic conductivity of $\text{Li}_{6.4}\text{Al}_{0.2}\text{La}_3\text{Zr}_2\text{O}_{12}$ garnet produced by solid-state synthesis. *RSC Adv.*, 2018, 8, Pages 13083–13088
12. M. Klementová. Electron diffraction – SAED, CBED, PED
13. X. Shi, W. Zhou, D. Ma. Electrospinning of Nanofibers and Their Applications for Energy Devices. *Journal of Nanomaterials*, Volume 2015, doi:10.1155/140716
14. Goodenough, J. B. and Park. The Li-Ion Rechargeable Battery: A Perspective. *J. Am. Chem. Soc.* 135, 2013, Pages 1167–1176.
15. A. Alyamani and O.M. Lemine. FESEM characterization of some nanomaterial. March 2012, doi: 10.5772/343361
16. M.J. Piernas and E.C. Martinez. Introduction to batteries. In: Prussian Blue Based Batteries. *SpringerBriefs in Applied Sciences and Technology*. doi:10.1007/978-3-319-914888-6_1
17. Q. Zhao, S. Stalin and C. Zhao. Designing solid-state electrolytes for safe, energy-dense batteries. *Nature Reviews Materials*, 2020, Volume 5, Pages 229 - 252
18. BU-808c: Coulombic and Energy Efficiency with the Battery. *Battery University*